

Quasi-Fermi liquid behavior in a one-dimensional system of interacting spinless fermions

Joshua D. Baktay,¹ Alexander V. Rozhkov²,³ Adrian E. Feiguin,¹ and Julián Rincón³

¹*Department of Physics, Northeastern University, Boston, Massachusetts 02115, USA*

²*Institute for Theoretical and Applied Electrodynamics, Russian Academy of Sciences, 125412 Moscow, Russia*

³*Department of Physics, Universidad de los Andes, Bogotá D.C. 111711, Colombia*

 (Received 16 June 2023; revised 4 November 2023; accepted 20 November 2023; published 12 December 2023)

We present numerical evidence for a paradigm in one-dimensional interacting fermion systems, whose phenomenology has traits of both Luttinger liquids and Fermi liquids. This state, dubbed a *quasi-Fermi liquid*, possesses a discontinuity in its fermion occupation number at the Fermi momentum. The excitation spectrum presents particlelike quasiparticles and absence of holelike quasiparticles, giving rise instead to edge singularities. Such a state is realized in a one-dimensional spinless fermion lattice Hamiltonian by fine-tuning the interactions to a regime where they become irrelevant in the renormalization group sense. We show, using uniform infinite matrix products states and finite-entanglement scaling analysis, that the system ground state is characterized by a Luttinger parameter $K = 1$ and a discontinuous jump in the fermion occupation number. We support the characterization with calculations of the spectral function that show a particle-hole asymmetry reflected in the existence of well-defined Landau quasiparticles above the Fermi level and edge singularities without the associated quasiparticles below. These results indicate that the quasi-Fermi liquid paradigm can be realized beyond the low-energy perturbative realm.

DOI: [10.1103/PhysRevB.108.245134](https://doi.org/10.1103/PhysRevB.108.245134)

I. INTRODUCTION

It is well understood that a fairly generic, interacting quantum system in one spatial dimension (1D) can be described at low energies by Luttinger liquid (LL) theory [1]. This proposal overrules the standard Fermi liquid (FL) theory due to the reduced phase-space scattering between particles, preventing the formation of quasiparticles and forcing instead the existence of collective excitations [2,3]. The conventional LL paradigm involves linearizing the dispersion relation around the Fermi surface, which consists of two points. This approximation is justified because the band curvature is irrelevant in the renormalization group sense for energy scales arbitrarily close to the Fermi level. Indeed, spectral function calculations are asymptotically exact but only in the low-energy, perturbative regime [4–11]. However, capturing more realistic physics requires accounting for irrelevant interactions at higher energy scales where linearization is no longer appropriate [9–19].

Attempting to apply LL theory at high energies unavoidably leads to modifications, giving rise to unexpected behavior that defies common knowledge. Phenomenology beyond this “linear” LL paradigm include considering corrections to the theory around a stable fixed point that can be associated to (i) the curvature of the dispersion relation, (ii) irrelevant interactions, or (iii) a momentum-dependent interaction potential [8–11,16,17,20,21].

In a FL, irrelevant terms can be accounted for perturbatively. They broaden the spectral function, maintaining the quasiparticle picture. This perturbation-theory approach fails in LL theory. For example, at finite dispersion curvature, the Lorentz invariance and particle-hole symmetry introduced by the linearization are both broken, leading to on-shell divergences [16,17]. Together, these symmetry breaking effects

lift the degeneracy in the dispersion relation leading to qualitatively new behavior in the dynamic correlations [12,15]. The differences are twofold. (1) Near the Fermi momentum, k_F , the spectral functions of both the linear and nonlinear LLs possess power-law singularities but with different scaling exponents [16,17]. (2) Away from k_F , the excitation spectrum can develop finite lifetime quasiparticles or power-law excitations [11,16,19,20].

We present a microscopic, spinless fermion model that, contrary to the conventional paradigms, simultaneously exhibits both FL and LL characteristics. This *quasi-Fermi liquid* (qFL) was originally presented in Refs. [13,18] in the context of a 1D continuum Hamiltonian that contains only irrelevant interactions, with scaling dimension three. The model was found to realize a discontinuity in the momentum distribution while lacking the perturbatively defined fermionic quasiparticles normally indicated by such a discontinuity. The former hints to FL behavior while the latter indicates LL behavior. We numerically study the ground state of the equivalent lattice problem directly in the thermodynamic limit using uniform matrix product states (uMPS) [22–25] and the variational uMPS (VUMPS) algorithm [25,26]. Our VUMPS results are further refined using finite-entanglement scaling (FES) [27–30]. Evidence for the qFL is further strengthened by characterizing the excitation spectrum using large-scale time-dependent density matrix renormalization group (tDMRG) calculations [31–34].

The main goal of this work is to show, using uMPS, VUMPS, FES, and tDMRG, that the universality class defined by the qFL paradigm can be detected in the nonperturbative regime in quantum lattices. This is accomplished by analyzing the ground and excited states of a lattice Hamiltonian at different fillings such that the ground state exhibits FL behavior,

while the excitation spectrum suggests similarities with the nonlinear LL. This physics is realized along a critical line with Luttinger parameter $K = 1$ in Hamiltonian parameter space, legitimizing the departure from the standard LL and FL paradigms of quantum fluids.

The article below has the following structure. In Sec. II, we introduce our model and the relevant numerical methods. In Sec. III, the momentum distribution and the charge static structure factor are computed and analyzed for evidence of both FL and LL behavior. This is followed by calculations of the spectral function in both the particle and hole sectors, as well as a scaling analysis of various momentum cuts. We close with a discussion of the results and their possible implications in Sec. IV.

II. MODEL AND METHODS

In this work we focus on a 1D, extended, spinless fermion model on the lattice with interactions to first and second neighbors. The Hamiltonian is written as

$$H = -t \sum_j (c_j^\dagger c_{j+1} + \text{H.c.}) + \mu \sum_j \tilde{n}_j + V \sum_j \tilde{n}_j \tilde{n}_{j+1} + V_2 \sum_j \tilde{n}_j \tilde{n}_{j+2}, \quad (1)$$

with $\tilde{n}_j = c_j^\dagger c_j - 1/2$ giving the particle-hole symmetric version at $\mu = 0$. Parameters V and V_2 are the nearest-neighbor and next-nearest-neighbor interactions, respectively, and μ is the chemical potential; all energies are expressed in units of the hopping t .

The phase diagram in the $V > 0$, $V_2 > 0$ region was characterized in Ref. [35] at half filling using finite-size DMRG. Four phases were identified: two charge-density-wave insulating phases, a LL phase, and a bond-order phase. The charge-density-wave regions arise when either V or V_2 (V' in their notation) is appreciably greater than the other. In between these two regions, where V and V_2 are comparable, there is a LL phase that transitions into the bond-order phase at higher values of V and V_2 .

According to Ref. [18], for a generic system of interacting fermions, the qFL state can be stabilized by fine-tuning the interaction couplings such that marginal interactions are nullified. The influence of relevant interactions such as umklapp, which occur at commensurate fillings, can be avoided by setting $\mu \neq 0$. The remaining *irrelevant* interactions stabilize this unique state. In our case, this involves tuning V and V_2 with the constraint $V \cdot V_2 < 0$; i.e., if one is attractive, the other is repulsive.

In order to account properly for the singular behavior of the 1D problem, it is necessary to resort to methods that work directly in the thermodynamic limit [36]. To this aim, the translationally invariant ground state is represented by a uMPS [22,23], characterized by its bond dimension, χ , which controls the size of its matrices and defines a variational manifold as a subspace of the exponentially large, many-body Hilbert space. The minimum within this manifold, with respect to the cost function $\langle \text{uMPS} | H | \text{uMPS} \rangle$, corresponds to the approximate ground state. It is reached via the DMRG-inspired VUMPS algorithm [26], which iteratively finds the

ground state and its energy, subject to an error threshold criterion. Convergence to a variational minimum is characterized by the energy density error and the norm of the tangent vector. Our simulations achieved energy density errors and tangent vector norms on the order of 10^{-12} and 10^{-13} , respectively. The quality of our uMPS approximation to the exact ground state wave function is captured by the discarded weight as a function of χ . Our simulations included bond dimensions up to $\chi = 640$ which yield discarded weights of the order of 10^{-10} . For more details on the VUMPS algorithm we refer the reader to Refs. [25,26].

By virtue of the translational invariance of our system, the uMPS ansatz works directly in the thermodynamic limit, thus removing any finite-size effects. However, uMPS are still approximate, though quasiexact, variational wave functions due to the finite bond dimension χ . Physically, χ captures the approximate amount of entanglement present in the system and can be tuned to improve accuracy. A finite χ introduces finite-entanglement effects analogous to finite-size effects. This can be overcome using a FES analysis, which allows one to extrapolate physical quantities of interest to the infinite-bond dimension limit, by analyzing its behavior against a suitable length scale parameter [27–30]. This FES analysis was done for all relevant expectation values to follow.

III. RESULTS

A. Ground state

The general characteristics of the FL can be understood in terms of the Landau conjecture, which states that the ground state and low-energy excited states of a FL are adiabatically connected to the free Fermi gas, exhibiting nonzero overlap between them. On the other hand, the ground and excited states of a LL have zero overlap with the noninteracting case, thus constituting their own universality class. For the qFL, because its usually dominant, marginal interactions have been nullified, one expects its ground state to be perturbatively connected to the ground state of the free Fermi gas. However, in the infrared limit, the remaining, technically irrelevant interactions now have nontrivial effects on its excited states; they have no fermionic quasiparticles, which implies no overlap with the noninteracting case, like a LL. (Indeed, one might instead expect bosonic excitations; see discussion below.)

According to the above argument, it is then natural to seek ground states that have a Luttinger parameter $K = 1$. Such parameter accounts for the nature and strength of the interaction in the LL. It follows from LL theory that K can be extracted as a low-momentum, linear approximation of the charge structure factor (CSF), the Fourier transform of the density-density correlation function,

$$D(k) = \sum_j \langle n_0 n_j \rangle e^{-ikj}. \quad (2)$$

The CSF was computed for the uMPS representing the ground state in the thermodynamic limit [25]. For known $D(k)$, the parameter K can be extracted from the slope near $k \rightarrow 0^+$: $dD(k)/dk = K/\pi$ [2,3,37]. A grid search was carried out through a wide range of the parameter space, depicted in Fig. 1, where a narrow band is seen whose values of V and V_2

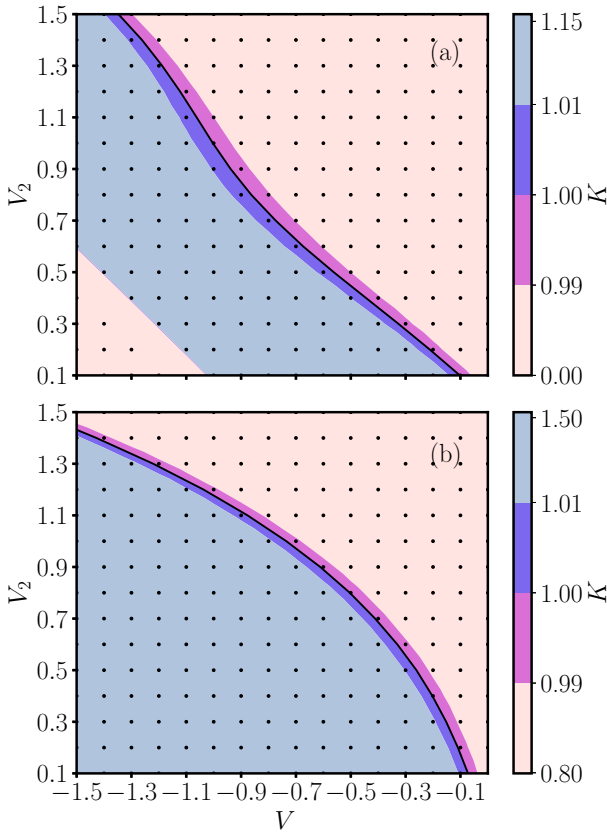


FIG. 1. Phase diagram of Luttinger parameter, K , for $V < 0$ and $V_2 > 0$ at $\mu/t = +1.0$ (a) and $\mu/t = +0.5$ (b). The quasi-Fermi liquid state is stable along the black curve which is our best estimate of the critical line, obtained as an interpolation of the data points within the band of qFL candidates, $0.99 < K < 1.01$. The band can be made arbitrarily precise with a step size $0 < \delta \leq 0.1$. Above this band the ground state is dominated by charge-ordered fluctuations. Below the band, the ground state is dominated by superconducting fluctuations [3]. For $\mu/t = +1.0$ (a) in the lower left corner, as V becomes much greater than V_2 the particles are driven into a very sparse, charge-ordered state. This breaks translation invariance which prevents ground state convergence resulting in the missing data points. Those that converge have $K \approx 0$.

yield $K \approx 1$. Crucially, these values of V, V_2 are generally comparable in magnitude but not perfectly equal, highlighting the importance of a judicious grid search. The pairs (V, V_2) , with fixed μ , represent a family of qFL candidates for further investigation.

In order to thoroughly characterize the state of matter emerging along the $K = 1$ line, as shown in Fig. 1, we now present a full analysis for two sets of representative parameter value candidates: $(V, V_2, \mu) \in \{(-0.6, 0.9, 0.5), (-1.0, 1.0, 1.0)\}$ [38].

The CSF for the two candidates we highlight can be seen in Fig. 2(a). The deviations at high momenta from the plateau-like trend of free fermions are a signature of interacting behavior. The overall smoothness of the curves indicates the absence of charge order. We point out that correlation functions can change significantly with χ (because of its approximate nature), revealing spikes in the CSF at higher χ in the presence

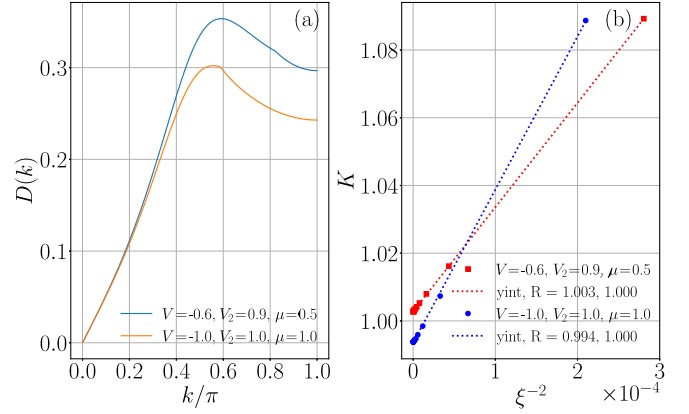


FIG. 2. Static charge structure factor $D(k)$ vs k (a) and the Luttinger parameter K vs ξ^{-2} (b) for two quasi-Fermi liquid candidates. Panel (a) contains a family of $D(k)$ curves, plotted for different values of χ , for each candidate. Individual curves in each family are not discernible due to the lack of change as χ increases (see main text). Panel (b) shows K in the infinite χ limit as the intercept of a linear fit. Our two candidates converge to $K = 1.0028$ and 0.9936 with statistical correlation $\simeq 1$.

of charge order. Here, we do not observe this behavior and instead conclude that the ground state is metallic.

We conducted a FES analysis to determine K for our candidates in the infinite-bond dimension limit, based on finite-bond dimension data. This is displayed in Fig. 2(b), where K is plotted versus the correlation length of the MPS, $\xi := \xi_1(\chi)$, defined as

$$\xi_1(\chi)^{-1} = -\ln|\lambda_1(\chi)|, \quad (3)$$

where $\lambda_1(\chi)$ is the second largest eigenvalue of the MPS transfer matrix [25,27–30]. A similar analysis can be done using the length scale $\delta = \xi_n^{-1} - \xi_1^{-1}$, in place of $\xi_1(\chi)$, where $\xi_n^{-1} = -\ln|\lambda_n(\chi)|$ and $\lambda_n(\chi)$ is the n th subleading eigenvalue of the MPS transfer matrix [29]; other combinations of ξ_n 's are also possible [30]. Indeed, we have found an analogous scaling behavior to that shown in Fig. 2(b) for two equivalent definitions: $\delta = \xi_2^{-1} - \xi_1^{-1}$ and $\delta = \xi_3^{-1} - \xi_1^{-1}$ (not shown) [38]. The length scales ξ and δ control the finite-entanglement scaling properties of the MPS approximation. It is expected that, as $\chi \rightarrow \infty$, both $\xi \rightarrow \infty$ and $\delta \rightarrow 0$. A linear fit yields an intercept value equal to the extrapolated value of K for $\xi \rightarrow \infty$. Given the high statistical correlation of the fit, we can be confident in the value of K and the legitimacy of the $K \approx 1$ band in parameter space.

Next, the momentum distribution function $n(k)$,

$$n(k) = \sum_j \langle c_0^\dagger c_j \rangle e^{-ikj}, \quad (4)$$

was calculated similarly to the CSF [25]. According to LL theory, $n(k)$ possesses a power-law singularity near the Fermi momentum k_F [1–3],

$$n(k) \sim \text{sgn}(k - k_F) |k - k_F|^{(K+K^{-1})/2-1}, \quad (5)$$

in sharp contrast to the discontinuity present in FL.

A finite bond dimension introduces an inherent length scale via the MPS correlation length, ξ , that limits the resolution

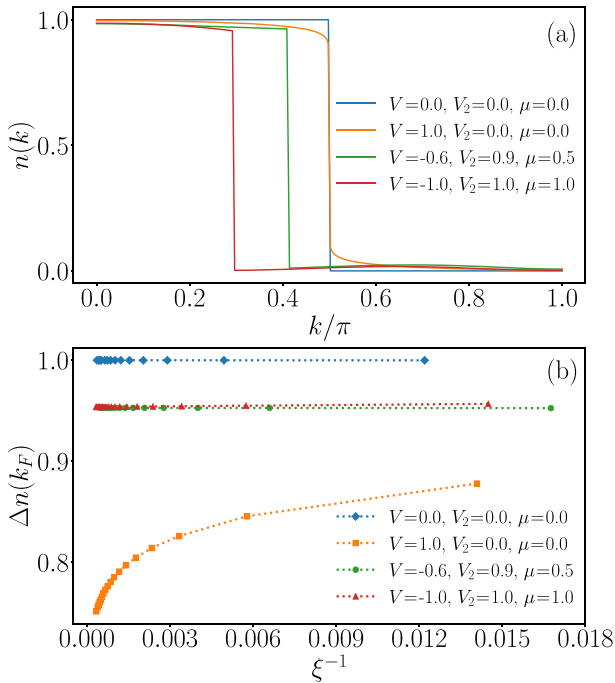


FIG. 3. Momentum distribution $n(k)$ vs k (a) and size of the discontinuity $\Delta n(k_F)$ vs ξ^{-1} (b) for both candidates compared to the free Fermi gas $(V, V_2) = (0, 0)$ (blue) and a known LL state $(V, V_2) = (1, 0)$ (yellow); clearly in panel (b) the scaling behavior of the LL differs greatly from the rest. The quasi-Fermi liquid candidates and the Fermi gas scale at most linearly, showing variations of order 10^{-3} whose intercept corresponds to $\Delta n(k_F)$ as $\chi \rightarrow \infty$. The Fermi gas converges to 1, as expected, while our candidates converge to ≈ 0.95 , thus demonstrating the presence of a true discontinuity. The LL scales logarithmically, implying the existence of a singularity at k_F . This is the expected power-law behavior, converging to zero for $\xi \rightarrow \infty$.

of all correlation functions and prevents one from easily discriminating between a singularity and a discontinuity in a finite-entanglement data set. Furthermore, extrapolating the numerical derivative at the k_F (using FES) cannot differentiate between FL and LL as the derivative of the LL power law also diverges at the Fermi momentum [36]. To overcome this, a FES analysis was performed on the size of the discontinuity about k_F computed as

$$\Delta n(k_F) \equiv n[k_F - \pi/\xi(\chi)] - n[k_F + \pi/\xi(\chi)], \quad (6)$$

with $\xi(\chi)$ defined above. The momentum distribution functions for our qFL candidates can be seen in Fig. 3(a). Discontinuity $\Delta n(k_F)$ versus correlation length can be seen in Fig. 3(b) compared against the Fermi gas and a known prototypical LL. Clearly the extrapolated behavior greatly differs between the two; the LL possesses a logarithmic scaling such that $\Delta n(k_F) \rightarrow 0$ as the correlation length increases, while the qFL displays at most a linear scaling such that $\Delta n(k_F)$ approaches a nonzero constant as $\xi(\chi) \rightarrow \infty$. This behavior matches that of the free Fermi gas, confirming our analysis. Other quantities such as the entanglement entropy of the ground state can also be readily obtained [38].

The jump in $n(k)$ together with $K = 1$, as $\xi \rightarrow \infty$, corroborates the FL behavior of our qFL ground state. However, the discontinuity in the momentum distribution cannot be interpreted in the usual way as evidence of perturbatively defined quasiparticles. The existence of quasiparticles is equivalent to the statement that the single-particle Green's function has poles with nontrivial residues (i.e., it possesses a quasiparticle weight $Z < 1$). According to Migdal's theorem, this form of the single-particle Green's function implies a discontinuity in the momentum distribution of the bare particles. However, the reverse is not necessarily correct: having a discontinuity in the momentum distribution does not imply the presence of a nontrivial residue in the single-particle Green's function and, therefore, the existence of quasiparticles. This is a necessary but not a sufficient condition for the presence of quasiparticles in the excitation spectrum of the system. Indeed, the discussion in Ref. [18] and its Supplemental Material indicates that, for qFL, the quasiparticle weight Z vanishes for holelike single-particle excitations at any finite momentum. This implies the lack of *fermionic holelike* quasiparticles in the low-lying excited states and thus the state with $K = 1$ is not merely a 1D FL.

B. Spectral function

An important quantity that can provide crucial information about the nature of the excitations in our 1D system is the single-particle spectral function:

$$A(k, \omega) = A_p(k, \omega) + A_h(k, \omega), \quad (7)$$

$$A_p(k, \omega) = \sum_{\alpha} |\langle \alpha | c_k^\dagger | 0 \rangle|^2 \delta(\omega - E_{\alpha} + E_0), \quad (8)$$

$$A_h(k, \omega) = \sum_{\alpha} |\langle \alpha | c_k | 0 \rangle|^2 \delta(\omega + E_{\alpha} - E_0), \quad (9)$$

which contains contributions from both the particle $A_p(k, \omega)$ and the hole $A_h(k, \omega)$ spectral functions. In these expressions $|0\rangle$ is the ground state of the system with N particles and ground state energy E_0 and the states $|\alpha\rangle$ are excited states with one extra particle or hole, $N \pm 1$, and energy E_{α} . In a free theory, the spectral function is given by a Dirac delta $A_p(k, \omega) \sim \delta(\omega - \epsilon_k)$, where ϵ_k is the dispersion relation. In the presence of interactions, FL theory dictates that the band curvature will be renormalized and peaks will now be broadened into Lorentzians, with a width determined by the quasiparticle lifetime. However, in 1D this picture breaks down due to the pervasive nesting and, instead, the low-energy physics is described by LL theory. In the particular soluble case of a linear dispersion, there is a particle-hole symmetry that is preserved and the excitation spectrum is a continuum with a power-law "edge singularity" given by

$$A(k, \omega) \sim \frac{\gamma_0^2}{(\omega - \epsilon_k)^{1-\gamma_0^2}} \theta[(\omega - \epsilon_k) \text{sgn } \epsilon_k], \quad (10)$$

where γ_0 is a constant that depends on the interaction potential [4–7, 14]. Notice that, while the particle (hole) spectrum diverges as one approaches the mass shell $\omega = \epsilon(k)$ from above (below), it also displays a sharp threshold or discontinuity on the opposite side. As previously pointed out, the presence of curvature in the dispersion ϵ_k or irrelevant interactions

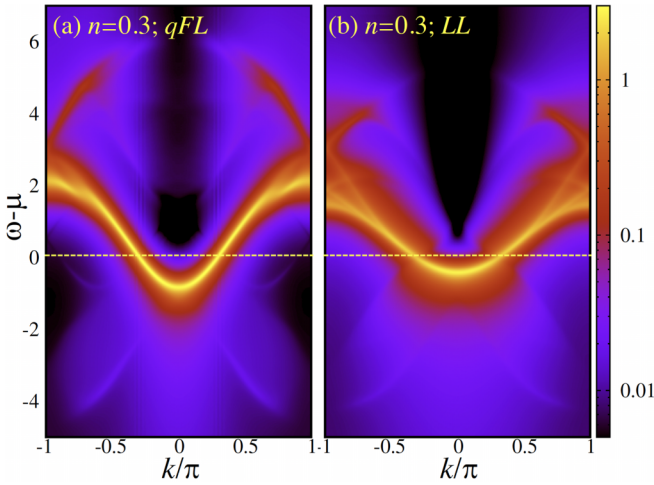


FIG. 4. Momentum resolved spectral function at density $n = 0.3$ in a logarithmic color scale for (a) a quasi-Fermi liquid with $(V, V_2) = (-1, 1)$ and (b) a Luttinger liquid with $(V, V_2) = (-1.5, 0)$. Dashed lines indicate the Fermi level, where $k_F/\pi = 0.3$. Notice the renormalization of the bandwidth for the quasi-Fermi liquid candidate, the particle-hole asymmetry, the faint continuum in the hole spectrum ($\omega < \mu$), and the high energy bound state on the particle side ($\omega > \mu$).

produce some quite dramatic effects [9–11,14,16,20]: due to the broken particle-hole symmetry, the spectral function in the particle sector, near k_F , now displays a Lorentzian peak near the mass shell $\omega = \epsilon_k$, a feature of a FL; away from ϵ_k , it displays an asymmetric two-sided power law. Notably, the spectral function in the hole sector still preserves the character of a LL.

In order to characterize the spectrum of our model we carry out large-scale tDMRG simulations on 1D chains. We consider systems with up to $L = 240$ sites using $m = 400$ DMRG states and a time step $\delta t = 0.05$. This guarantees a truncation error smaller than 10^{-7} for times up to $t_{\max} = 80$ (this implies that the main source of error stems from the Suzuki-Trotter decomposition). We follow the prescription detailed in Ref. [11] with minor modifications: to account for the open boundary conditions, we use a Hann window in real space that damps the effects of the edges and an exponential Hann window in time $w(t) = \exp(-\epsilon t)$, such that a Dirac delta peak would now have a Lorentzian line shape with an artificial broadening ϵ ,

$$A(\omega) \sim \frac{1}{\pi} \frac{\epsilon}{\omega^2 + \epsilon^2}. \quad (11)$$

As long as the interlevel spacing is much smaller than ϵ we should not expect noticeable finite-size effects [39,40]. If we assume that the bandwidth is $W \sim 4t$, the level spacing is of the order of $2W/L \sim 8t/L$.

We focus our study on the regime with density $n = 0.3$ with $(V, V_2) = (-1, 1)$, such that the band curvature $d^2\epsilon_k/dk^2 > 0$ at the Fermi level is more noticeable. To aid intuition, we first show the full momentum-resolved spectral function in Fig. 4, compared to that of a LL with the same density and $(V, V_2) = (-1.5, 0)$. The logarithmic scale allows us to clearly resolve the asymmetry between the particle

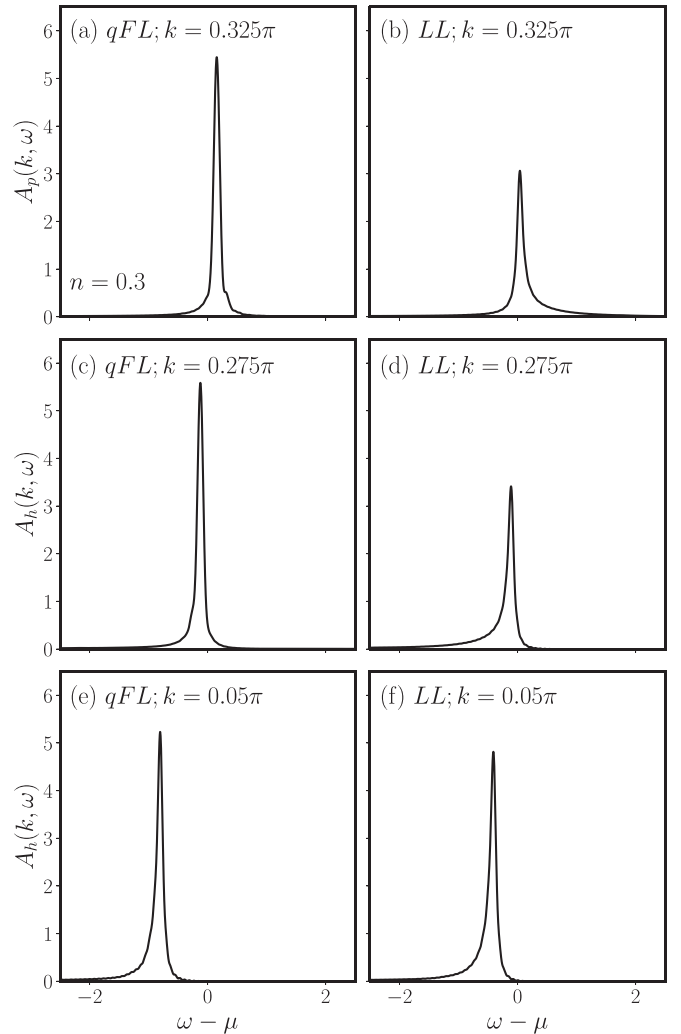


FIG. 5. Momentum cuts for the particle (a),(b) and hole (c)–(f) sectors of the spectral function at density $n = 0.3$, for several values of momentum near and away from the Fermi points, located at $k_F = 0.3\pi$. Left columns correspond to a quasi-Fermi liquid with $(V, V_2) = (-1, 1)$ and right columns to a Luttinger liquid with $(V, V_2) = (-1.5, 0)$. Results are obtained with an artificial broadening $\epsilon = 0.05$.

($\omega > \mu$) and hole ($\omega < \mu$) sectors, with an obvious broadening that increases with the distance from k_F and a high-energy branch near $k = \pi$ that can be associated to bound states [11]. Besides the obvious change in the effective mass and the bandwidth, the qFL may seem to possess a more coherent dispersion near k_F , as predicted using field-theory methods [13,18]. Regardless, for the hole spectrum we can observe a faint continuum that spreads to high energies in both cases shown.

We carry our study of the line shape near, and away from, the Fermi points as a function of the broadening ϵ . In Fig. 5 we show several cuts at fixed values of momenta for $\epsilon = 0.05$ (we point out that we avoid sitting exactly at $k = k_F$ because this is the “edge” of the particle/hole band and, due to the open boundary conditions and the Hann window used in the Fourier transform, results may be more affected). For the LL we observe a clear asymmetry resembling an edge singularity,

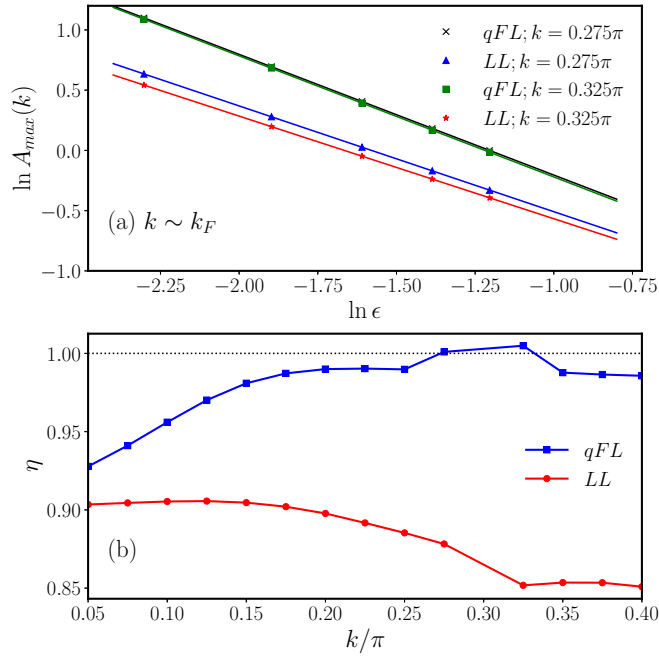


FIG. 6. (a) Scaling of the maximum in the spectral function for fixed values of k near k_F , for the particle ($k > k_F = 0.3\pi$) and hole ($k < k_F = 0.3\pi$) sectors, both for the quasi-Fermi liquid and the Luttinger liquid having density $n = 0.3$. (b) Power-law exponent obtained from the slopes in (a) for different values of momentum k .

while a similar asymmetry is evident for the qFL only at high energies, near the bottom of the band. The sharp peaklike structures displayed by the qFL at momenta $k \sim k_F$ may suggest the possibility of well-defined fermionic quasiparticles near the Fermi level. To extract more conclusive evidence, we first look at the scaling of the peak maximum A_{\max} as a function of $1/\epsilon$, as shown in Fig. 6(a) in a logarithmic scale. Following Ref. [41], a fit to a power law $A_{\max} \sim \epsilon^{-\eta}$ yields exponents $\eta = 1.001$ and $\eta = 1.004$ for $k = 0.325\pi$ and $k = 0.285\pi$, respectively, a strong indication that the peaks may be Lorentzians that evolve toward a Dirac delta in the limit $\epsilon \rightarrow 0$. These values give an interpolated $\eta \approx 1.002$ at k_F , suggesting an accuracy of at least 0.2%, taking into account that the values of V and V_2 had to be fine-tuned and there is an error stemming from this estimate as well. Notice that we avoid values of k too close to k_F to avoid artifacts created by the open boundary conditions and the Hann window [11]. This is in agreement with the fact that $K \approx 1$. In contrast, the results for the LL show that η differs noticeably from unity, and from each other, as expected from a power-law singularity edge. To validate this approach, we also fit the exponent for a LL at half filling with $(V, V_2) = (-1.5, 0)$: the Bethe-ansatz prediction is $\eta = 0.8416$ [11], while we obtain $\eta = 0.8262$ for $k = 0.475\pi$. In Fig. 6(b) we show the power-law exponent η as a function of momentum k obtained from the fits. Remarkably, for the qFL we see a clear change of behavior near the Fermi momentum, with the exponent approaching values very close to $\eta = 1$, suggesting that the FL-like behavior occurs only near the Fermi level.

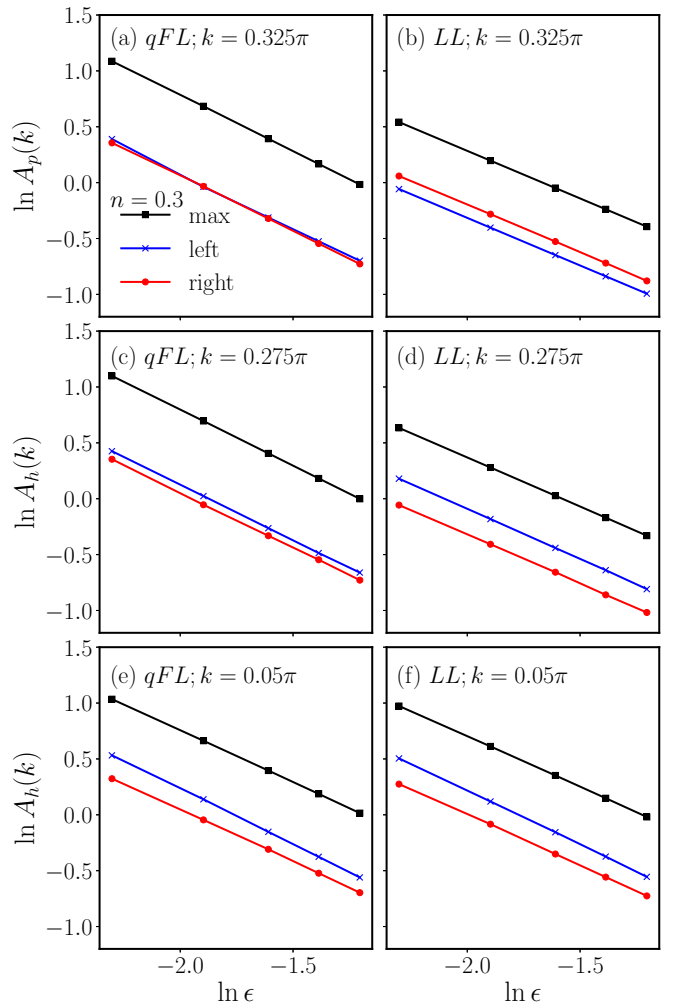


FIG. 7. Scaling of the maximum A_{\max} and the value of the spectral function at $\omega_{\max} \pm \epsilon$ for both the quasi-Fermi liquid and Luttinger liquid at density $n = 0.3$. We show results on the particle ($k > 0.3\pi$) and hole ($k < 0.3\pi$) sectors of the spectrum for some representative momenta k . Lines connecting the data points are a guide to the eye. The same scaling and symmetry in panel (a) are a strong indication of quasiparticle behavior.

To further characterize the singularities in the spectra, we plot the weight of the line shape at $\omega_{\max} \pm \epsilon$, where ω_{\max} is the position of the maximum, A_{\max} . If the scaling is the same as that of A_{\max} , and there is no left/right asymmetry, the evidence in favor of a Dirac delta pole is strengthened. As seen in Fig. 7, where we show representative data, this occurs on the particle sector of the spectrum, although the evidence weakens on the hole side due to an apparent asymmetry that grows with distance from k_F . This asymmetry, more dramatic for small k , is already present in the LL for all values of k , a hallmark of an edge singularity. To corroborate this behavior we also show in Fig. 8 the half width of the peak, measured to the left and to the right of the maximum $\sigma_{\pm} = |\omega_{\pm} - \omega_{\max}|$, where ω_{\pm} is the value of frequency at half maximum, $A(k, \omega_{\pm}) = A_{\max}/2$ from above and below. For an ideal Lorentzian, the points should lie on a straight line with slope 1, as it occurs in panel (a) for the qFL for $k \gtrsim k_F$. Once again, this points to the presence of a

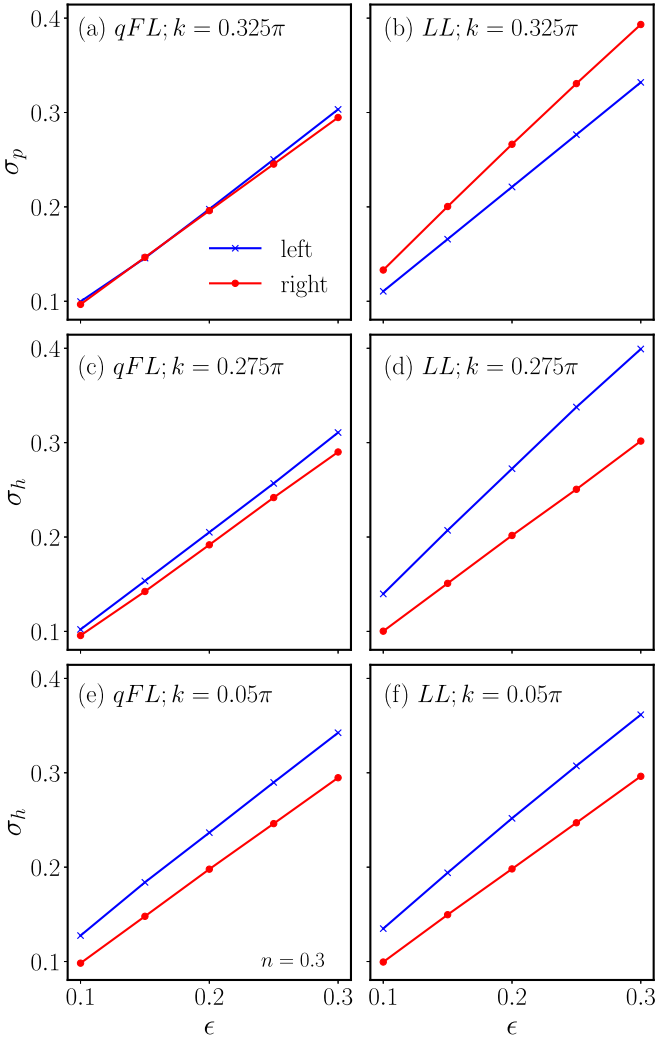


FIG. 8. Distance of the half maximum $A_{\max}/2$ from the position of the peak at ω_{\max} , for both the quasi-Fermi liquid and Luttinger liquid, at density $n = 0.3$. Lines connecting the data points are a guide to the eye. The linear scaling with slope one and the left/right symmetry in panel (a) are strong indications of quasiparticle behavior.

Dirac delta peak in the particle spectral function, but an edge singularity in the hole sector that broadens with an exponent η that decreases as one moves away from k_F .

If indeed the system realizes full fledged Landau quasiparticles, one should be able to associate the magnitude of the discontinuity in $n(k)$ with the quasiparticle weight $Z = |\langle N + 1 | c_k^\dagger | 0 \rangle|^2$. Due to the open boundary conditions, we use “particle-in-a-box” states [41]

$$c_k^\dagger = \sqrt{\frac{2}{L+1}} \sum_{\ell} \sin(k\ell) c_\ell^\dagger, \quad (12)$$

with $k = \pi\ell/(L+1)$, for integers $1 \leq \ell \leq L$. An extrapolated value of this quantity to the thermodynamic limit yields a value $Z = 0.945$ (not shown), which can be compared to the value of the pole in the spectral function at $k = 0.325\pi$, $Z = 0.940$. Conversely, the value of the discontinuity in Fig. 3(a) is 0.953, sufficiently close to support our conclusion.

IV. SUMMARY AND CONCLUSION

We have presented numerical evidence for the existence of the qFL state in 1D, which departs from both the standard LL and FL phenomenologies, and yet combines features from each. We achieved this in a spinless fermion lattice Hamiltonian system, by effectively nullifying the marginal interactions such that the remaining *irrelevant* interactions manifest in the state. We observed this for Hamiltonian parameters well beyond the perturbative regime, demonstrating the stability and legitimacy of the quasi-Fermi liquid state as a distinct metallic state of matter in one spatial dimension.

The continuum limit of our lattice model with generic V and V_2 interactions corresponds to an effective low-energy theory with marginal density-density interactions and additional irrelevant terms. From there, one may elect to drop these irrelevant terms leading to the typical linear LL model. Notably, what we have effectively done is nullify the marginal interaction while keeping the irrelevant terms. In our lattice Hamiltonian we have accomplished this by judiciously selecting values of (V, V_2, μ) , such that $K = 1$. This should account for retaining the irrelevant terms but “dropping” the marginal interactions. According to Ref. [18], the qFL paradigm states that irrelevant modifications to the noninteracting theory qualitatively change the nature of the ground state and excitations in the system.

Specifically, the qFL ground state is perturbatively connected to the free-fermion ground state as for the FL. This is evident from $n(k)$, shown in Fig. 3, due to the finite discontinuity in $n(k = k_F)$ and the renormalization of the occupations: $n(k \lesssim k_F) < 1$ and $n(k \gtrsim k_F) > 0$. As for excited states, certainly, the divergent quasiparticle residue Z in the hole sector implies that the excited states of a qFL are qualitatively different compared to those of free fermions.

As for excited states, the evidence presented here suggests that the spectral characteristics of the qFL should partly mimic those of the LL, but with well-defined fermionic quasiparticles for the addition spectrum A_p near the Fermi momentum k_F . In this regime the particlelike excitations resemble FL quasiparticles. On the other hand, the removal spectrum A_h displays edge singularities, which are asymptotically close to a Dirac delta as k approaches k_F , signaling the absence of holelike quasiparticles. These collective excitations are characteristic of LL. See Figs. 5–8.

The role of the particle and hole sectors for $A(k, \omega)$ can be swapped via a particle-hole transformation. Therefore, it is possible to realize quasiparticles for $|k| < k_F$ and edge singularities for $|k| > k_F$. In this work, we have studied the case when $k_F < \pi/2$ ($\mu > 0$). Conversely, we can understand the $k_F > \pi/2$ ($\mu < 0$) case by exchanging particles and holes.

The need for fine-tuning the marginal interactions originates from the fact that, without such a dominating term, the system stabilizes (flows to) a different phase: the qFL. This is how we understand the results of Fig. 1: above or below the $K = 1$ line in the phase diagram, marginal interactions dominate yielding either a repulsive, charge-ordered phase ($K < 1$) where V_2 dominates or an attractive, superconducting-like phase ($K > 1$) where V dominates. For the $K = 1$ line, marginal interactions are functionally not present and

the irrelevant terms secure the qFL phase, away from the low-energy perturbative regime.

There are other contexts where the qFL can be realized, apart from the competition between nearest- and next-nearest-neighbor interactions ($V \approx -V_2$), discussed in this work, for example, in Hamiltonian models that include next-nearest-neighbor and correlated hopping terms. Note, also, that the constraint $V \approx -V_2$ is not necessary for the stabilization of the state [38]. Hence we hypothesize that lattice Hamiltonians with general quartic interactions, beyond the nullification of marginal terms, are candidates to exhibit a qFL phase [42]. These conclusions might be extended to spinful fermions [19].

Lastly, we would like to note that a strict fine-tuning of the interactions is not necessary. As discussed in Sec. III, satisfying $|K - 1| < \delta$, where $\delta \ll 1$, is enough to detect the qFL signatures in the momentum distribution and the spectral

function. Thus an experimental realization could potentially not be as demanding. For instance, the qFL may be realized in optical lattice setups of fully polarized fermions, where fine control of interactions can systematically be engineered [43,44].

ACKNOWLEDGMENTS

A.E.F. and J.D.B. acknowledge support from the U.S. Department of Energy, Office of Basic Energy Sciences under Grant No. DE-SC0014407. J.R. acknowledges support from the Office of the Vice-president of Research and Creative Activities and the Office of the Faculty of Science Vice-president of Research of Universidad de los Andes under the FAPA grant. J.D.B. thanks P. Weinberg for valuable interactions at the initial stages of developing the MPS code.

-
- [1] F. D. M. Haldane, Luttinger liquid theory of one-dimensional quantum fluids. 1. Properties of the Luttinger model and their extension to the general 1D interacting spinless Fermi gas, *J. Phys. C* **14**, 2585 (1981).
 - [2] A. O. Gogolin, A. A. Nersisyan, and A. M. Tsvelik, *Bosonization of Strongly Correlated Systems* (Cambridge University Press, Cambridge, UK, 1998).
 - [3] T. Giamarchi, *Quantum Physics in One Dimension* (Oxford University Press, Oxford, 2003).
 - [4] I. Dzyaloshinskii and A. I. Larkin, Correlation functions for a one-dimensional Fermi system with long-range interaction (Tomonaga model), *Zh. Eksp. Teor. Fiz.* **65**, 41 (1973) *Sov. Phys. JETP* **38**, 202 (1974)].
 - [5] A. Luther and I. Peschel, Single-particle states, Kohn anomaly, and pairing fluctuations in one dimension, *Phys. Rev. B* **9**, 2911 (1974).
 - [6] V. Meden and K. Schönhammer, Spectral functions for the Tomonaga-Luttinger model, *Phys. Rev. B* **46**, 15753 (1992).
 - [7] J. Voit, Charge-spin separation and the spectral properties of Luttinger liquids, *Phys. Rev. B* **47**, 6740 (1993).
 - [8] K. Schönhammer and V. Meden, Nonuniversal spectral properties of the Luttinger model, *Phys. Rev. B* **47**, 16205 (1993).
 - [9] A. Imambekov and L. I. Glazman, Phenomenology of one-dimensional quantum liquids beyond the low-energy limit, *Phys. Rev. Lett.* **102**, 126405 (2009).
 - [10] A. Imambekov and L. I. Glazman, Universal theory of nonlinear Luttinger liquids, *Science* **323**, 228 (2009).
 - [11] R. G. Pereira, S. R. White, and I. Affleck, Spectral function of spinless fermions on a one-dimensional lattice, *Phys. Rev. B* **79**, 165113 (2009).
 - [12] M. Pustilnik, M. Khodas, A. Kamenev, and L. I. Glazman, Dynamic response of one-dimensional interacting fermions, *Phys. Rev. Lett.* **96**, 196405 (2006).
 - [13] A. V. Rozhkov, Class of exactly soluble models of one-dimensional spinless fermions and its application to the Tomonaga-Luttinger Hamiltonian with nonlinear dispersion, *Phys. Rev. B* **74**, 245123 (2006).
 - [14] M. Khodas, M. Pustilnik, A. Kamenev, and L. I. Glazman, Fermi-Luttinger liquid: Spectral function of interacting one-dimensional fermions, *Phys. Rev. B* **76**, 155402 (2007).
 - [15] R. G. Pereira, S. R. White, and I. Affleck, Exact edge singularities and dynamical correlations in spin-1/2 chains, *Phys. Rev. Lett.* **100**, 027206 (2008).
 - [16] A. Imambekov, T. L. Schmidt, and L. I. Glazman, One-dimensional quantum liquids: Beyond the Luttinger liquid paradigm, *Rev. Mod. Phys.* **84**, 1253 (2012).
 - [17] R. G. Pereira, Long time correlations of nonlinear Luttinger liquids, *Int. J. Mod. Phys. B* **26**, 1244008 (2012).
 - [18] A. V. Rozhkov, One-dimensional fermions with neither Luttinger-liquid nor Fermi-liquid behavior, *Phys. Rev. Lett.* **112**, 106403 (2014), see also Supplemental Material.
 - [19] F. H. L. Essler, R. G. Pereira, and I. Schneider, Spin-charge-separated quasiparticles in one-dimensional quantum fluids, *Phys. Rev. B* **91**, 245150 (2015).
 - [20] L. Markhof and V. Meden, Spectral function of the Tomonaga-Luttinger model revisited: Power laws and universality, *Phys. Rev. B* **93**, 085108 (2016).
 - [21] V. Meden, Nonuniversality of the one-particle Green's function of a Luttinger liquid, *Phys. Rev. B* **60**, 4571 (1999).
 - [22] G. Vidal, Classical simulation of infinite-size quantum lattice systems in one spatial dimension, *Phys. Rev. Lett.* **98**, 070201 (2007).
 - [23] J. Haegeman, J. I. Cirac, T. J. Osborne, I. Pižorn, H. Verschelde, and F. Verstraete, Time-dependent variational principle for quantum lattices, *Phys. Rev. Lett.* **107**, 070601 (2011).
 - [24] U. Schollwöck, The density-matrix renormalization group in the age of matrix product states, *Ann. Phys. (NY)* **326**, 96 (2011).
 - [25] L. Vanderstraeten, J. Haegeman, and F. Verstraete, Tangent-space methods for uniform matrix product states, *SciPost Phys. Lect. Notes* **7** (2019).
 - [26] V. Zauner-Stauber, L. Vanderstraeten, M. T. Fishman, F. Verstraete, and J. Haegeman, Variational optimization algorithms for uniform matrix product states, *Phys. Rev. B* **97**, 045145 (2018).
 - [27] L. Tagliacozzo, T. R. de Oliveira, S. Iblisdir, and J. I. Latorre, Scaling of entanglement support for matrix product states, *Phys. Rev. B* **78**, 024410 (2008).
 - [28] F. Pollmann, S. Mukerjee, A. M. Turner, and J. E. Moore, Theory of finite-entanglement scaling at one-dimensional

- quantum critical points, *Phys. Rev. Lett.* **102**, 255701 (2009).
- [29] M. M. Rams, P. Czarnik, and L. Cincio, Precise extrapolation of the correlation function asymptotics in uniform tensor network states with application to the Bose-Hubbard and XXZ models, *Phys. Rev. X* **8**, 041033 (2018).
- [30] B. Vanhecke, J. Haegeman, K. Van Acoleyen, L. Vanderstraeten, and F. Verstraete, Scaling hypothesis for matrix product states, *Phys. Rev. Lett.* **123**, 250604 (2019).
- [31] S. R. White and A. E. Feiguin, Real-time evolution using the density matrix renormalization group, *Phys. Rev. Lett.* **93**, 076401 (2004).
- [32] A. J. Daley, C. Kollath, U. Schollwöck, and G. Vidal, Time-dependent density-matrix renormalization-group using adaptive effective Hilbert spaces, *J. Stat. Mech.: Theory Exp.* **2004**, P04005 (2004).
- [33] A. E. Feiguin, The density matrix renormalization group method and its time-dependent variants, in *Lectures on the Physics of Strongly Correlated Systems XV-Fifteenth Training Course in the Physics of Strongly Correlated Systems*, AIP Conf. Proc. No. 1419 (AIP, Melville, NY, 2011), pp. 5–92.
- [34] S. Paeckel, T. Köhler, A. Swoboda, S. R. Manmana, U. Schollwöck, and C. Hubig, Time-evolution methods for matrix-product states, *Ann. Phys. (NY)* **411**, 167998 (2019).
- [35] T. Mishra, J. Carrasquilla, and M. Rigol, Phase diagram of the half-filled one-dimensional t - V - V' model, *Phys. Rev. B* **84**, 115135 (2011).
- [36] C. Karrasch and J. E. Moore, Luttinger liquid physics from the infinite-system density matrix renormalization group, *Phys. Rev. B* **86**, 155156 (2012).
- [37] S. Daul and R. M. Noack, Ferromagnetic transition and phase diagram of the one-dimensional Hubbard model with next-nearest-neighbor hopping, *Phys. Rev. B* **58**, 2635 (1998).
- [38] See Supplemental Material at <http://link.aps.org/supplemental/10.1103/PhysRevB.108.245134> for general results in the regime ($V > 0, V_2 < 0$) and additional results on finite-entanglement scaling analysis and ground-state entanglement entropy. The Supplemental Material also contains Refs. [45–47].
- [39] E. Jeckelmann, Dynamical density-matrix renormalization-group method, *Phys. Rev. B* **66**, 045114 (2002).
- [40] M. Paech and E. Jeckelmann, Blind deconvolution of density-matrix renormalization-group spectra, *Phys. Rev. B* **89**, 195101 (2014).
- [41] H. Benthien, F. Gebhard, and E. Jeckelmann, Spectral function of the one-dimensional Hubbard model away from half filling, *Phys. Rev. Lett.* **92**, 256401 (2004).
- [42] J. D. Baktay *et al.* (unpublished).
- [43] T. Esslinger, Fermi-Hubbard physics with atoms in an optical lattice, *Annu. Rev. Condens. Matter Phys.* **1**, 129 (2010).
- [44] F. Schäfer, T. Fukuhara, S. Sugawa, Y. Takasu, and Y. Takahashi, Tools for quantum simulation with ultracold atoms in optical lattices, *Nat. Rev. Phys.* **2**, 411 (2020).
- [45] C. Holzhey, F. Larsen, and F. Wilczek, Geometric and renormalized entropy in conformal field theory, *Nucl. Phys. B* **424**, 443 (1994).
- [46] G. Vidal, J. I. Latorre, E. Rico, and A. Kitaev, Entanglement in quantum critical phenomena, *Phys. Rev. Lett.* **90**, 227902 (2003).
- [47] P. Calabrese and J. Cardy, Entanglement entropy and quantum field theory, *J. Stat. Mech.: Theory Exp.* (2004) P06002.